NMR study of defect-induced magnetism in methylammonium lead iodide perovskite

Bilwadal Bandyopadhyay,[1,*] Homnath Luitel,[2,3,†] Sayantan Sil,[4] Joydeep Dhar,[5] Mahuya Chakrabarti,[6] Palash Nath,[7] Partha P. Ray,[4] and Dirtha Sanyal[2,3,‡]

[1]*Saha Institute of Nuclear Physics, 1/AF Bidhannagar, Kolkata-700064, India*
[2]*Variable Energy Cyclotron Centre, 1/AF, Bidhannagar, Kolkata 700064, India*
[3]*Homi Bhabha National Institute, Training School Complex, Anushakti Nagar, Mumbai 400094, India*
[4]*Department of Physics, Jadavpur University, Kolkata 700032, India*
[5]*Department of Chemistry, Birla Institute of Technology, Mesra, Ranchi 835215, India*
[6]*Department of Physics, Basirhat College, Basirhat 743412, India*
[7]*Department of Physics, Kaliyaganj College, Kaliyaganj 733129, India*

(Received 10 June 2019; revised manuscript received 23 January 2020; accepted 27 February 2020; published 16 March 2020)

In organic-inorganic perovskite semiconductor methylammonium lead iodide the occurrence of magnetism has been confirmed from magnetization and ^{1}H nuclear magnetic resonance (NMR) measurements. From room temperature down to 4 K, the magnetization is a combination of weak ferromagnetism and paramagnetism. ^{1}H NMR spectra at low temperatures also reveal two components, one with a small chemical shift characteristic of ^{1}H resonance in nonmetals, and the other with a much larger shift of ~ -100 ppm that is ascribed to the ferromagnetism of the material. The analysis of NMR spectra as well as that of ^{1}H spin-lattice relaxation rate ($1/T_1$) indicates that disorder produces an inhomogeneous distribution of magnetic moments that order ferromagnetically where they are dense enough and otherwise behave as random paramagnetic impurities. It is shown that magnetism arises from iodine and lead vacancies present in the orthorhombic and cubic crystal phases of the material.

DOI: 10.1103/PhysRevB.101.094417

I. INTRODUCTION

Methylammonium lead iodide, a hybrid perovskite with chemical formula $CH_3NH_3PbI_3$, is well known in the field of optoelectronics for its excellent photovoltaic properties [1–6]. Extraordinary optical and electronic properties like very low exciton binding energy [3], slow charge recombination kinetics [7], strong optical absorption [8], large exciton diffusion length [4], high charge carrier mobility [5], etc., transpire into almost 100% internal quantum efficiency [9] leading to a very high (>25%) photovoltaic efficiency [10]. Rotational motion of organic cation is believed to be the origin of polar nature of hybrid perovskites [11,12]. Several studies have demonstrated that these materials behave as mixed electronic-ionic conductors and lattice defects mediated ionic motion may also govern their dipolar nature [13]. Recent studies [14,15] have established that ionic conductivity arises from defects in the form of intrinsic cationic ($CH_3NH_3^+$; henceforth labeled as MA^+) and anionic (I^-) vacancies.

In the present work, we report an experimental observation of room temperature ferromagnetism through magnetization and ^{1}H NMR measurements in polycrystalline $MAPbI_3$. Theoretical analysis employing DFT calculations suggests that the origin of ferromagnetic ordering is in atomic defects. As for applications of this material, optically tuned magnetic switches were reported [16] with $MAPbI_3$ after extrinsically doping Mn^{2+} in place of Pb^{2+} in crystal lattice. Recently, utilizing the strong spin-orbit coupling, two spintronic-based devices, viz., a 'spin light emitting diode' and a 'vertical spin valve' with giant magnetoresistance have been demonstrated [17]. Ferroelectricity has been identified to play a crucial role in exciton generation and creation of free charge carriers upon absorption of light [11,18]. Therefore, the present observation of intrinsic ferromagnetism in a direct band gap semiconductor like $MAPbI_3$ should provide a real boost for its potential in the field of multiferroics for spintronic application.

The samples used in this study were prepared by mechanochemical process from CH_3NH_3I and PbI_2. The details of synthesis, characterization, and defect studies were described earlier [14,15]. In addition in the present study, a defectless single crystalline $MAPbI_3$ sample was also prepared. From measurement of magnetic field dependence of magnetization at room temperature it was verified that the single crystalline sample as well as the initial ingredients CH_3NH_3I and PbI_2 were diamagnetic with a magnetic susceptibility of $\sim -1.0 \times 10^{-4}$ emu/mol. It was a confirmation that the magnetism that is reported here is intrinsic to $CH_3NH_3PbI_3$ and not due to any extraneous magnetic impurities.

*bilwadal.bandyopadhyay@saha.ac.in
†Present address: Department of Physics, Sikkim Government College, Namchi-737126, India
‡dirtha@vecc.gov.in

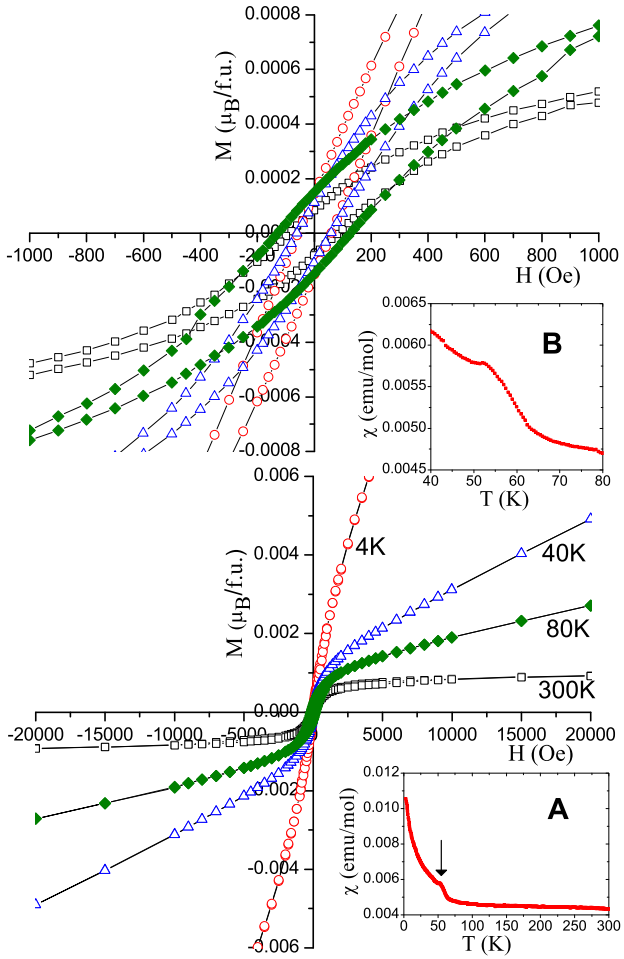

FIG. 1. The bottom figure shows the full range of magnetic field (H) dependence of magnetization (M) at different temperatures as indicated. The top figure shows the same plots expanded around the origin. The lower inset 'A' shows the temperature dependence of bulk magnetic susceptibility (χ) measured at 500 Oe. The arrow indicates the region of a 'weak' maximum that is shown in expanded scale in upper inset 'B.'

II. RESULTS AND DISCUSSION

A. Magnetization studies

The magnetization measurements were performed using a superconducting quantum interference device vibrating sample magnetometer (SQUID-VSM) of Quantum Design. Figure 1 shows the magnetic field (H) dependence of magnetization (M) at various temperatures 4–300 K. The plots show that from room temperature down to 4 K, M is a combination of two components; a ferromagnetic (FM) one with a hysteresis and a coercive field of about 100 Oe, and a linear paramagnetic component. Accordingly, the data of M vs H at different temperatures have been analyzed [19,20]. The results, given in Table I, show that the ferromagnetic saturation magnetization M^{FM} is orders of magnitude stronger than the paramagnetic susceptibility, χ_{para}. From room temperature down to ~80 K, both χ_{para} and M^{FM} show a small and gradual increase. A larger variation is obtained at lower temperatures. Between 80 and 4 K, M^{FM} increases by a factor of two, and χ_{para} increases by an order of magnitude. The same magnetization behavior is reflected also in the temperature dependence of total magnetic susceptibility χ, obtained from M vs T measured at 500 Oe, shown in inset 'A' of Fig. 1. There is an interesting feature in the rapidly increasing part of χ below ~60 K, i.e., a 'weak' maximum which is shown prominently in inset 'B' of Fig. 1. The occurrence of such a feature will be investigated later.

TABLE I. Ferromagnetic saturation magnetization (M^{FM}) and linear magnetic susceptibility (χ_{para}) of $MA\mathrm{PbI_3}$ obtained from the analysis of magnetization data at different temperatures.

Temp (K)	M^{FM} (emu/mol)	χ_{para} (emu/mol)
300	4.45(5)	$3.6(5) \times 10^{-5}$
80	6.15(5)	$4.6(5) \times 10^{-4}$
40	7.25(5)	$10.0(5) \times 10^{-4}$
4	13.25(5)	$4.7(5) \times 10^{-3}$

B. Nuclear magnetic resonance (NMR) measurements

1. ^{1}H *NMR spectra*

The magnetism of $MA\mathrm{PbI_3}$ has been further investigated by nuclear magnetic resonance (NMR) spectroscopy with a Bruker 300 MHz Ultrashield magnet and Thamway PROT4103MR spectrometer. A good ^{1}H NMR signal was obtained by simply using a two turn silver coil for rf excitation, i.e., tuning and matching capacitors were absent. The spectra at various temperatures 4–296 K were recorded by sweeping the rf in 5 kHz steps over the position of ^{1}H resonance by applying a $\frac{\pi}{2}$-τ-$\frac{\pi}{2}$-solid-echo pulse sequence with an appropriate phase cycling. A rather long $\frac{\pi}{2}$ pulse of 100 μs was used to minimize broadening during integration of spin echo signals. At higher temperatures the spectra were obtained from Fourier transformation of the free-induction decay (FID) signal by exciting the whole spectrum at once with a much shorter $\frac{\pi}{2}$ pulse.

Figure 2 shows the ^{1}H spectra of $MA\mathrm{PbI_3}$ at different temperatures 4–296 K. Near room temperature the low frequency shift and width (full width at half maximum, ~25 ppm) of the resonance line is of the order of the inhomogeneity of the external magnetic field. The lineshape is Lorentzian with a slight asymmetry. With the lowering of temperature, the spectra showed an apparent shift towards lower frequency and clearly revealed an asymmetric broadening, which could not be accounted for by incorporating chemical shift anisotropy. Below ~150 K, the spectra could be satisfactorily simulated as a sum of two components; one with a small low frequency shift as before which is designated as component 'A' and another Gaussian resonance component with a larger low frequency shift, denoted as component 'B.' The simulations are also shown in Fig. 2. Figure 3 shows the temperature dependence of shifts of the two components and their corresponding linewidths. Both the components exhibit a pronounced broadening only at low temperatures below ~40 K. The component A appears to be in the same position irrespective of temperature. The low frequency shift of component B shows a pronounced temperature dependence. The variation of the

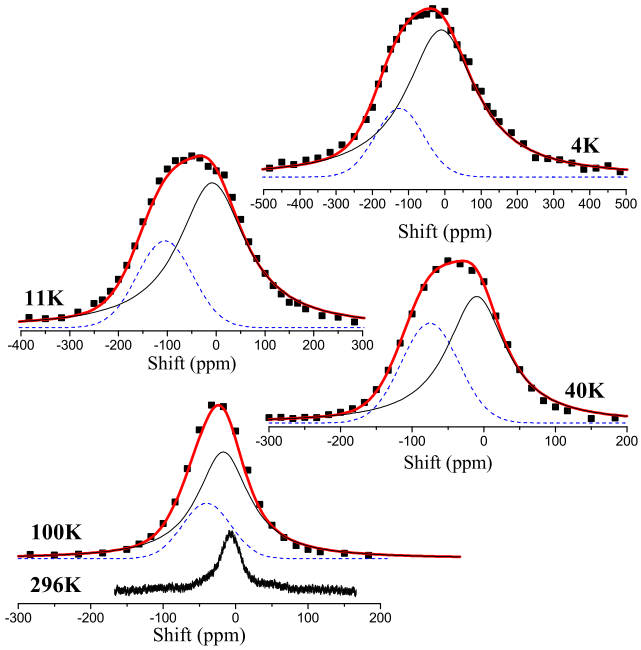

FIG. 2. ^{1}H NMR spectra of *MA*PbI$_3$ at different temperatures and their simulation as described in the text. The thin solid and broken lines indicate the resonance components, 'A' and 'B,' respectively, and the thick line denotes their sum.

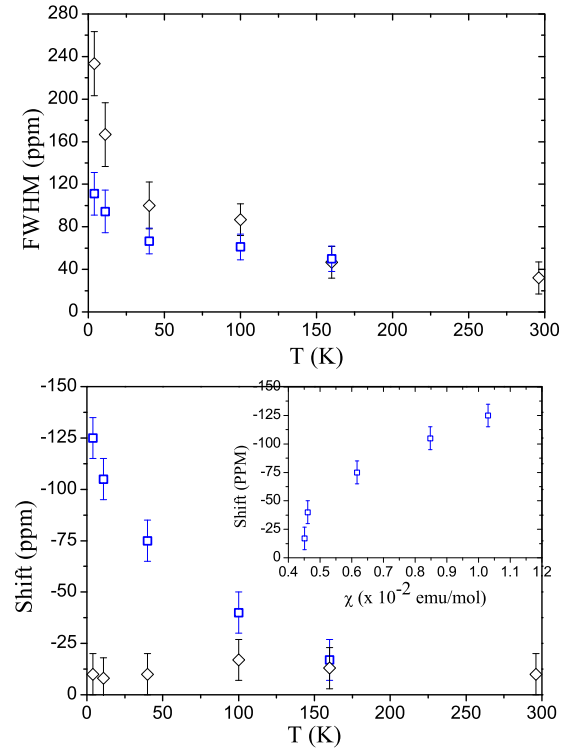

FIG. 3. Temperature dependence of shift (bottom figure) and full width at half maximum (FWHM, top figure) of ^{1}H NMR spectral components of *MA*PbI$_3$. The symbols are: (◇) for component A and (□) for component B. For the latter, the inset shows the variation of shift with the magnetic susceptibility (χ) with temperature as the intrinsic parameter. The external magnetic field inhomogeneity is ∼10 ppm.

shift of component B with the bulk magnetic susceptibility (χ) is also shown in the inset of Fig. 3(a).

In ^{1}H NMR experiments, the shift in the resonance frequency is determined by the hyperfine field produced at the nucleus of H by the 1*s* electrons. Usually in nonmetallic systems, ^{1}H shift is very small, a few ppm only. However, the shift can be larger if there is *s*-electron polarization in the presence of electronic magnetism in the system. Such a polarization usually produces a negative shift in the resonance frequency. The linewidth of the resonance spectrum is determined by the time-averaged fluctuation of the local field which is a sum of the dipolar and the hyperfine field. It may be mentioned here that extraneous magnetic impurities, in principle, may give rise to a broadening of NMR spectrum, especially at very low temperatures. However, it is the shift of the NMR spectrum which firmly establishes the intrinsic magnetic nature of the system. Overall, by comparing the analyses of magnetization data and NMR spectra, it is reasonable to argue that the NMR spectrum component having the larger shift, i.e., component A results from ferromagnetism of *MA*PbI$_3$ while component B corresponds to ^{1}H in paramagneticlike *MA*PbI$_3$.

2. ^{1}H *spin-lattice relaxation rate*

The time dependence of local field fluctuations determines the ^{1}H spin-lattice relaxation rate ($1/T_1$) which was measured in between 80–300 K using the saturation-recovery method. Initially, the equilibrium ^{1}H nuclear magnetization $\mathcal{M}_\infty$ is in the direction of external magnetic field taken as H_z. Using an appropriate pulse sequence, $\mathcal{M}_\infty$ is rotated to the *xy* plane by applying a $\frac{\pi}{2}$ pulse, and then the recovery of $\mathcal{M}$ to equilibrium is monitored at variable times τ_d. Since the two spectral components have large overlap at all temperatures, we used a $\frac{\pi}{2}$ pulse of high power and short duration to excite sufficiently the central part of the spectrum. It followed that the recovery of magnetization was not exponential. In order to analyze the data we considered the following.

In a system of an inhomogeneous distribution of local magnetic moments, the time dependence of $\mathcal{M}_\tau$ should ideally be a combination of multiple exponentials. In such systems if nuclear spin diffusion is not important, $\mathcal{M}_\tau$ can be expressed as a stretched exponential of the form $\mathcal{M}_\tau = \mathcal{M}_0[1 - \exp(-\tau/T_1)^\beta]$, where $0.5 \leqslant \beta \leqslant 1.0$. More specifically, stretched exponential relaxation behavior can be seen as equivalent to a smooth distribution of relaxation times reflecting the magnetic inhomogeneity of the system [21]. However, when there is strong dipolar coupling, as in the case of nuclear spins with large magnetic moments like ^1H, the spin-diffusion process becomes effective and the nuclei relax predominantly due to dipolar interaction with local electronic spin moments. In that case, magnetization recovery approaches an exponential law, i.e., β in the above equation becomes ≈1. In other words, stretched relaxation behavior is not usually expected in spin-lattice relaxation time measurements in strongly coupled nuclear spin systems even in the presence of magnetic inhomogeneity. However, such behavior was found out in ^1H spin systems when magic angle spinning (MAS) technique was used to average out the dipolar interaction [22].

In the present case, $\mathcal{M}_\tau$ vs τ_d data for the wide range of τ_d values ranging from $\tau_d < 10^{-3}$ s to $\tau_d > 1$ s could not be described by the stretched exponential behavior written in the above-mentioned form. On the other hand, the data for $60 \leqslant T \leqslant 240$ K were fitted quite satisfactorily to an expression of a sum of two exponential components as

$$1 - \mathcal{M}(\tau_d)/\mathcal{M}_\infty = \mathcal{M}_s \exp(-\tau_d/T_{1s}) + \mathcal{M}_l \exp(-\tau_d/T_{1l}) \quad (1)$$

where $\mathcal{M}_s$ and $\mathcal{M}_l$ are the equilibrium magnetizations corresponding to the two components with different relaxation times, T_{1s} and T_{1l}, respectively, with $T_{1s} < T_{1l}$. The data and the fit at certain different temperatures are shown in Fig. 4. The good quality of fit over the entire range of τ_d values from $\sim 10^{-4}$ s to a few seconds confirms that the relaxation data can be adequately expressed as a combination of two distinct exponential components in the form of Eq. (1).

The analysis yields [20] that T_{1s} and T_{1l} correspond to two widely different ranges of values, i.e., $6 \lesssim T_{1s} \lesssim 30$ ms and 200 ms $\lesssim T_{1l} \lesssim 2$ s. The component with the faster relaxation rate $1/T_{1s}$ has smaller magnitude $\mathcal{M}_s$, and within the errors of estimation $1/T_{1s}$ appears almost temperature independent (Fig. S2(a), Ref. [20]). This component is therefore associated with the ferromagnetic component B in the spectra. The other component with slower relaxation rate $1/T_{1l}$ is associated with the larger spectral component A that is nearer to the reference position in the spectra (Fig. 2) and considered paramagnetic. Combining the analysis of spectra and spin-lattice relaxation time measurements, the NMR experiments therefore corroborate the results of magnetization measurements, both showing the existence of two different magnetization components and the occurrence of ferromagnetism near room temperature.

Figure 4(b) shows the temperature dependence of $1/T_{1l}$. It increases slowly with decrease in temperature initially, and then below $\sim$120 K it increases rapidly. Also, there appears a maximum of $1/T_{1l}$ around 80 K.

The enhancement of nuclear spin lattice relaxation rate (Γ_1) caused by dipolar interaction with electronic moments can be expressed in the form [23]

$$\Gamma_1 = \mathcal{C}r^{-6} \frac{\tau_c}{1 + \omega_I^2 \tau_c^2} \quad (2)$$

where ω_I is the nuclear Larmor frequency, and $\mathcal{C}r^{-6}$ is the electron-nuclear dipolar interaction derived under condition that dipole interaction vectors are rigid in the molecular frame. Here, $1/\tau_c$, the correlation rate, is given as $1/\tau_c = 1/\tau_r + 1/\tau_s$ where τ_r is the rotational correlation time of molecule and τ_s the electron relaxation time. Iwahara *et al.* [24] have shown that if the dipole-dipole interaction vectors within a large molecule are not rigid in the molecular frame, then Γ_1 is modified as

$$\Gamma_{1m} = \mathcal{S}^2 \mathcal{C}r^{-6} \frac{\tau_c}{1 + \omega_I^2 \tau_c^2} + (1 - \mathcal{S}^2)\mathcal{C}r^{-6} \left[\frac{\mathcal{S}^2 \tau_c}{1 + \omega_I^2 \tau_c^2} + \frac{(1 - \mathcal{S}^2)\tau_t}{1 + \omega_I^2 \tau_t^2} \right] \quad (3)$$

where $\mathcal{S}^2$ is the generalized order parameter reflecting the rigidity of intramolecular bonds, and $1/\tau_t = 1/\tau_c + 1/\tau_i$ incorporates the correlation time τ_i of internal motion. It has been shown [24] that for an order parameter $\mathcal{S}^2$ of 0.5, Γ_1 of

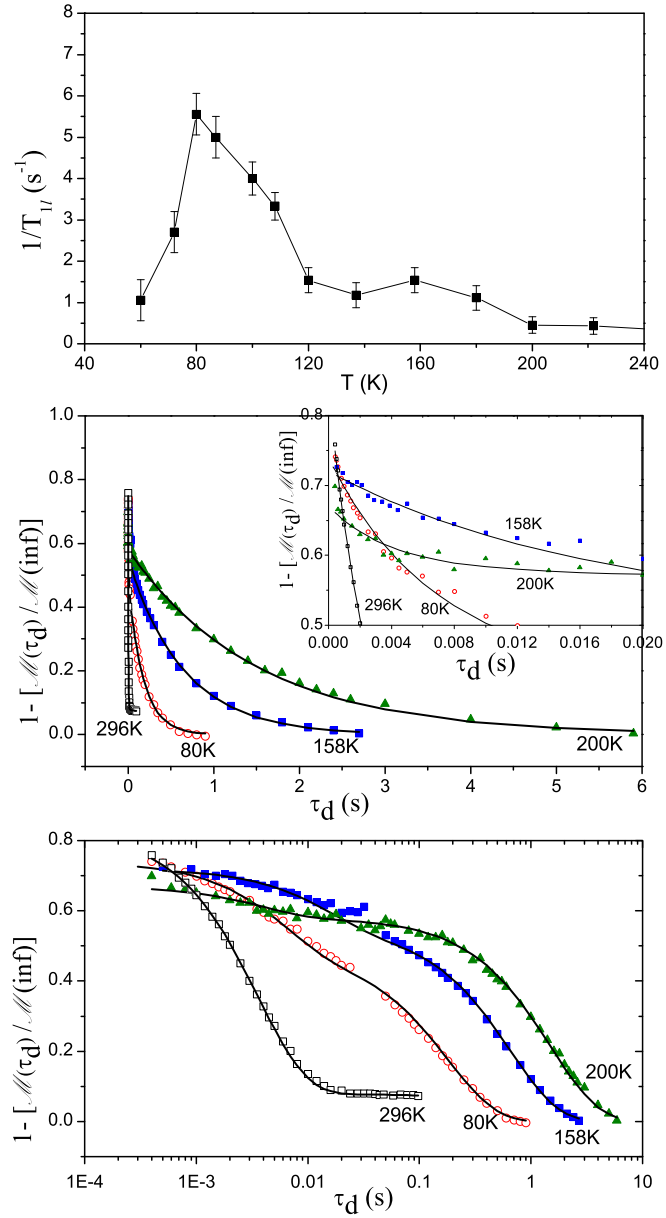

FIG. 4. In the bottom panel, the discreet points are experimental data in the measurement of ^{1}H spin-lattice relaxation time (T_1) at different temperatures and the solid lines are fit to Eq. (1). The logarithmic x axis has been used to show the quality of fit over the whole range covering four orders of magnitude of τ_d. The middle panel and its inset show the same fit using linear x axes for expanded long and short τ_d ranges, respectively. The top panel shows the temperature dependence of the slower component $1/T_{1l}$ of ^{1}H spin-lattice relaxation rate. The line is to guide the eye.

^1H in large organic molecules exhibits a strong dependence on τ_i showing a maximum around $\tau_i = 1/\omega_I$, with a value that is about five times Γ_1 in the absence of internal motion. The maximum appears even for larger values of $\mathcal{S}^2$, i.e., in relatively rigid molecules. Therefore, the observed peak in $1/T_{1l}$ possibly indicates that MAPbI$_3$ molecule experience bond fluctuations even far below the room temperature, at the rate of the order of ω_I at $\sim$80 K.

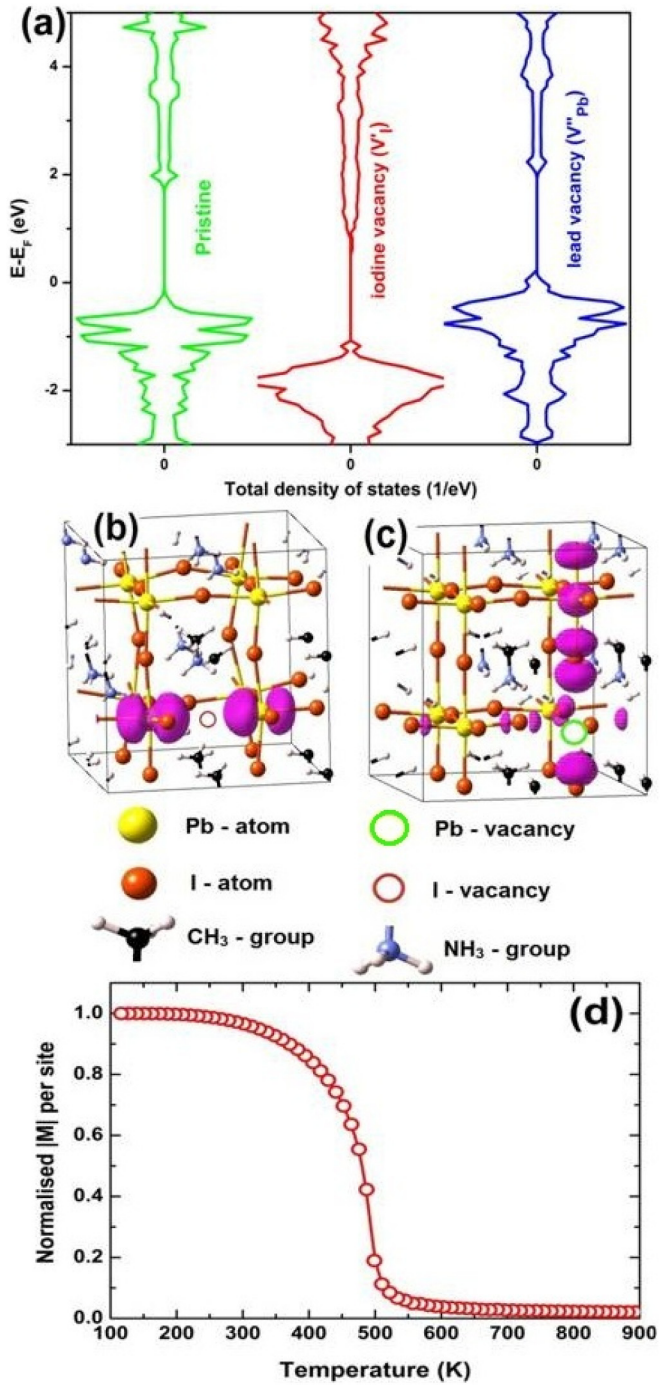

FIG. 5. For the cubic phase of MAPbI$_3$: (a) the spin polarized density of states for a pristine system and with defects $V_I^{\bullet}$ and V''_{Pb}, (b) and (c) spin polarized magnetization density (shown as lobes) for $V_I^{\bullet}$ and V''_{Pb}, respectively, (d) normalized magnetization (M) vs temperature (T) obtained using Monte Carlo simulation.

A significant change occurs in the ^{1}H relaxation behavior above ∼270 K. Here, a rapid relaxation process with $T_1 \sim$ 0.005 s dominates the whole of ^{1}H nuclear magnetization. It probably signifies the onset of rapid H motion in the MA^+ group [25] resulting in the averaging of ^{1}H nuclear dipolar interactions and the consequent enhancement of spin-lattice relaxation rate. The temperature induced dynamic processes in the MA^+ group in MAPbI$_3$ may have time scales of the order of picoseconds or even smaller [25] and are too fast to be studied by NMR spectroscopy. However, the magnetism of MAPbI$_3$ does not involve MA^+ group, as we will see below, and therefore doesn't get affected by the motion.

III. THEORY

In order to theoretically understand the origin of magnetism, the spin polarized density of states (DOS) calculations were carried out with VASP code [26–29] built in MedeA software package with the PAW pseudopotential, combining with generalized gradient approximation and Perdew-Burke-Ernzerhof exchange and correlation methods [30]. In a supercell system of $2 \times 2 \times 2$ unit cells of cubic MAPbI$_3$, calculations were for: (i) a pristine system, (ii) a system with one iodine vacancy ($V_I^{\bullet}$), and (iii) a system with one lead vacancy (V''_{Pb}), the latter two being the so-called 'defects.' Similar calculations were carried out for the two other possible crystal structures of MAPbI$_3$, viz., orthorhombic and tetragonal.

As shown in Fig. 5(a), the pristine system has a symmetric spin polarized DOS, i.e., there is equal up and down spin electrons distribution, and hence, the system is diamagnetic. In the presence of $V_I^{\bullet}$ and V''_{Pb}, the total DOS becomes asymmetric resulting in a net magnetic moment in the system. The generation of $V_I^{\bullet}$ and V''_{Pb} each imparts a magnetic moment of ∼0.7 μ_B in the cubic system. In the tetragonal structure no magnetic moment is generated by any atomic vacancies but the iodine vacancy ($V_I^{\bullet}$) in the orthorhombic structure also produces a magnetic moment of ∼0.74 μ_B. This observation explains the origin of magnetism in a mixed phase of these systems. The Pb atoms present in the vicinity of I vacancy give rise to the magnetic moment as shown in the magnetization density distribution [Fig. 5(b)] while the iodine atoms surrounding the Pb vacancy serve as a source of magnetism [Fig. 5(c)]. For a nominal defect concentration of 1% the magnetization of the sample turns out to be ∼44 emu/mol.

According to the DFT calculations, the free energy for the ferromagnetic ground state with iodine vacancy is ∼18.9 meV lower than its corresponding antiferromagnetic state in the cubic system and the spin-spin interaction strength comes out to be 9.45 meV. With these results, a numerical Ising model simulation has been performed for the magnetization properties of cubic spin lattice using the Metropolis algorithm on $16 \times 16 \times 16$ spin sites. Initially the system is thermalized for 10^4 Monte Carlo steps and then the collected data is averaged out for next 10^4 Monte Carlo steps. The temperature dependence of magnetization yields a Curie temperature of about ∼500 K as shown in Fig. 5(d).

IV. CONCLUSION

In summary, the measurement of bulk magnetization as well as investigations by NMR as a local probe reveal ferromagnetism in methylammonium lead iodide. First principle calculations using density functional theory suggest that iodine and lead vacancies are the primary source of magnetism in cubic crystal system of MAPbI$_3$ and only iodine vacancies in the orthorhombic system.

ACKNOWLEDGMENTS

The work was supported by Dept. of Atomic Energy (DAE), Govt. of India. S.S. acknowledges University Grants Commission (UGC), India, for providing a NET Senior Research Fellowship.

[1] W. E. I. Sha, X. Ren, L. Chen, and W. C. H. Choy, Appl. Phys. Lett. **106**, 221104 (2015).
[2] W. S. Yang, B.-W. Park, E. H. Jung, N. J. Jeon, Y. C. Kim, D. U. Lee, S. S. Shin, J. Seo, E. K. Kim, J. H. Noh, and S. I. Seok, Science **356**, 1376 (2017).
[3] V. D'Innocenzo, G. Grancini, M. J. P. Alcocer, A. R. S. Kandada, S. D. Stranks, M. M. Lee, G. Lanzani, H. J. Snaith, and A. Petrozza, Nat. Commun. **5**, 3586 (2014).
[4] Q. Dong, Y. Fang, Y. Shao, P. Mulligan, J. Qiu, L. Cao, and J. Huang, Science **347**, 967 (2015).
[5] R. L. Milot, G. E. Eperon, H. J. Snaith, M. B. Johnston, and L. M. Herz, Adv. Funct. Mater. **25**, 6218 (2015).
[6] T. M. Brenner, D. A. Egger, L. Kronik, G. Hodes, and D. Cahen, Nat. Rev. Mater. **1**, 15007 (2016).
[7] M. B. Johnston and L. M. Herz, Acc. Chem. Res. **49**, 146 (2016).
[8] M. A. Green, Y. Jiang, A. M. Soufiani, and A. Ho-Baillie, J. Phys. Chem. Lett. **6**, 4774 (2015).
[9] B. Yang, O. Dyck, J. Poplawsky, J. Keum, A. Puretzky, S. Das, I. Ivanov, C. Rouleau, G. Duscher, D. Geohegan, and K. Xiao, J. Am. Chem. Soc. **137**, 9210 (2015).
[10] NREL: National center for photovoltaics home page, https://www.nrel.gov/pv/assets/images/efficiency-chart.png (accessed).
[11] S. Liu, F. Zheng, N. Z. Koocher, H. Takenaka, F. Wang, and A. M. Rappe, J. Phys. Chem. Lett. **6**, 693 (2015).
[12] A. Stroppa, C. Quarti, F. D. Angelis, and S. Picozzi, J. Phys. Chem. Lett. **6**, 2223 (2015).
[13] W. Tress, J. Phys. Chem. Lett. **8**, 3106 (2017).
[14] J. Dhar, S. Sil, A. Dey, P. P. Ray, and D. Sanyal, J. Phys. Chem. Lett. **8**, 1745 (2017).
[15] J. Dhar, S. Sil, A. Dey, D. Sanyal, and P. P. Ray, J. Phys. Chem. C **121**, 5515 (2017).
[16] B. Nafradi, P. Szirmai, M. Spina, H. Lee, O. V. Yazyev, A. Arakcheeva, D. Chernyshov, M. Gibert, L. Forro, and E. Horvath, Nat. Commun. **7**, 13406 (2016).
[17] J. Wang, C. Zhang, H. Liu, R. McLaughlin, Y. Z. nad S. R. Vardeny, X. Liu, S. McGill, D. Semenov, H. Guo, R. Tsuchikawa, V. V. Deshpande, D. Sun, and Z. V. Vardeny, Nat. Commun. **10**, 129 (2019).
[18] L. M. Garten, D. T. Moore, S. U. Nanayakkara, S. Dwaraknath, P. Schulz, J. Wands, A. Rockett, B. Newell, K. A. Persson, S. Trolier-McKinstry, and D. S. Ginley, Sci. Adv. **5**, eaas9311 (2019).
[19] S. Dhara, R. R. Chowdhury, S. Lahiri, P. Ray, and B. Bandyopadhyay, J. Magn. Magn. Mater. **374**, 647 (2015).
[20] See Supplemental Material at http://link.aps.org/supplemental/10.1103/PhysRevB.101.094417 for (1) analysis of M vs H data, and, (2) temperature dependences of T_{1s}, T_{1l}, and $\mathcal{M}_s/(\mathcal{M}_s + \mathcal{M}_l)$.
[21] V. F. Mitrovic, M.-H. Julien, C. de Vaulx, M. Horvatic, C. Berthier, T. Suzuki, and K. Yamada, Phys. Rev. B **78**, 014504 (2008).
[22] S. Hayashi and E. Akiba, Sol. St. Nucl. Mag. Reson. **4**, 331 (1995).
[23] I. Solomon and N. Bloembergen, J. Chem. Phys. **25**, 261 (1956).
[24] J. Iwahara, C. D. Schwieters, and G. M. Clore, J. Am. Chem. Soc. **126**, 5879 (2004).
[25] J. M. Frost and A. Walsh, Acc. Chem. Res. **49**, 528 (2016).
[26] G. Kresse and J. Hafner, Phys. Rev. B **47**, 558 (1993).
[27] G. Kresse and J. Hafner, Phys. Rev. B **49**, 14251 (1994).
[28] G. Kresse and J. Furthmuller, Comput. Mater. Sci. **6**, 15 (1996).
[29] G. Kresse and J. Furthmuller, Phys. Rev. B **54**, 11169 (1996).
[30] J. P. Perdew, K. Burke, and M. Ernzerhof, Phys. Rev. Lett. **77**, 3865 (1996).